Investigating the Effects of Pre-Pretensioning on Occupant Kinematics and Abdominal Organ Response during Pre-Crash and In-Crash

Anurag Soni, Stefan Schilling and Andreas Lucht

Abstract While pre-crash braking reduced organ injury risk in animals in sled-testing, it is known to increase occupant forward excursion during pre-crash, thereby increasing risk of injurious interactions with vehicle interior in crashes. The combined use of pre-crash braking, like Autonomous Emergency Braking (AEB), with pre-pretensioner (PPT) might reduce both risks. The study objective, therefore, was to quantify reductions in forward excursions and loading on liver and spleen using simulations. The detailed GHBMC-M50 model was positioned in a simplified sled and restrained by a standard three-point belt system with a pyro-pretensioner and a 4 kN load limiter. Three cases of full-frontal impact at 56 kph were simulated: without AEB and PPT (0 g+0 N); AEB without PPT (1 g+0 N); and with AEB and 350 N PPT (1 g+350 N). The results showed that a standard belt system during AEB in 1 g+0 N reduced inertial load on liver and spleen, but resulted in higher forward excursion compared to no AEB in 0 g+0 N. Adding PPT counteracted occupant's forward motion during AEB in 1 g+350 N and held it in upright posture before the crash. Inertial loading on both organs was reduced against 0 g+0 N, but was higher compared to 1 g+0 N. Therefore, PPT appeared to reduce abdominal organ loading without compromising forward excursion.

Keywords Abdominal organ response, GHBMC model, in-crash, pre-crash braking, pre-pretensioner.

I. INTRODUCTION

Seat belts decrease automobile-related fatalities and injuries [1-2]. They mitigate the high forces inflicted on the occupants during a crash by firmly restraining the occupant's pelvis, clavicle and rib cage, thereby restricting occupant motion within the vehicle such that the risk of injurious interactions with interior components is minimised. To ensure the optimum coupling between the occupant and the decelerating vehicle, the restraining process must begin early in the crash. Any slack in the seat belt delays the coupling and eventually degrades the system performance [3]. Seat-belt pyro-pretensioners are used to eliminate belt slack almost immediately after sensing the crash [4-5].

Despite improvements in occupant coupling with seat belt, some human body parts are still not adequately restrained. These include the head, extremities (arms and legs), and internal organs with surrounding soft tissues. The viscoelastic characteristics of human tissues [6] result in these structures requiring a certain amount of displacement before experiencing resistive forces from the connecting body structures. This could be conceived as functional slack in the human body, which initially delays the onset of acceleration but ultimately leads to increased acceleration. This phenomenon is particularly apparent with externally visible body parts, such as when the extremities and/or head are thrown forward in a sled test with cadavers or in sled simulations with human body models (HBMs). Although not visible externally, this phenomenon is also expected to occur with inner organs, especially abdominal solid organs like liver and spleen. Several studies have shown that liver and spleen undergo substantial movement during postural changes [7-8] and when the abdomen is directly loaded [9-13], while deformation in the neighbouring hollow organs or soft tissues may allow more displacement.

Reducing viscoelastic functional slack in the human body can provide additional protective benefits, much like eliminating belt slack. In a series of sled test studies using baboon cadavers and human volunteers [14-15] in the early 1980s, the imposition of pre-impact braking on the sled showed potential benefits in this context. In these studies, subjects in both the test series were restrained with belts. The animal surrogates were exposed to pre-braking deceleration ranging from 0.2 g to 0.3 g, with maximum sled acceleration of 50 g, while human

Dr A. Soni (e-mail: anurag.soni@autoliv.com; tel: +49-41217975620), S. Schilling and A. Lucht work at Autoliv North Germany.

volunteers were subjected to pre-braking deceleration of 0.25 g and 0.62 g, with maximum sled acceleration of 8 g and 10 g. The results of the animal surrogate study demonstrated that pre-impact sled deceleration notably reduced severe injuries sustained by the animals compared to an equivalent impact without pre-impact deceleration. Specifically, out of six matched pairs of tests, only one case of severe injury occurred with imposed deceleration, compared to four cases without it, which included one case of liver tear. Similarly, the human volunteer tests showed significant reduction in measured chest and head accelerations with pre-impact deceleration. It was postulated that the imposed deceleration led to inertially induced dynamic preload in the body parts, which helped them rearrange and reduce the slack before impact, thereby preventing amplified accelerations during the impact phase and reducing the likelihood of severe injuries. Although the test studies were conducted in a military/aerospace context, the loading and restraint conditions used in these tests were not different from those encountered in automotive crashes. Therefore, the conclusions drawn from these studies remain relevant and applicable in the context of automotive safety.

However, the implementation of pre-crash braking technology got delayed due to the lack of necessary sensing devices. The concept of integrated safety was first proposed in the early 2000s [16], offering an Autonomous Emergency Braking (AEB) system combined with reversible pre-pretensioners. With the advancement in sensor technology, the AEB systems became more effective and sophisticated, leading to their mandatory inclusion in all new car models in the European Union from 2022, with the requirement extending to all new registrations from 2024 [17]. Studies have shown that in real-world accidents, AEB systems have been effective in reducing the severity of accidents and the resulting injuries by slowing down the vehicle before the collision [18-19]. From a restraint system standpoint, however, a downside of the pre-crash braking action has been identified, in that it can cause occupants to move forward into a suboptimal body position [20-21], which can increase the risk of injury to the head [22-23].

Restraint systems adapting to these postural changes may prevent the likelihood of severe injuries [22]. Systems such as seat-belt pre-pretensioner (PPT) can be activated in the pre-crash phase (or even before any occupant movement) if an imminent crash is identified in advance by sensors using e.g. radar or video systems [23]. While PPT systems tighten the seat belt and reduce belt slack in the pre-crash phase, they can significantly reduce the forward excursions and can even reposition the occupants to their nominal position [23-24]. Moreover, reducing occupant forward displacement by pre-pretensioning in combination with the reduced impact speed due to AEB might reduce injury risks even further than AEB alone [24-25].

While the previous sled test studies revealed that pre-crash braking can mitigate injury severity by reducing the inner body slack and improving coupling among body parts, however, it is also identified that such braking may lead to unfavourable occupant position before the crash, thereby increasing the risk of injury. The combined use of pre-crash braking and PPT could be beneficial in mitigating both of the risks. Therefore, the objective of this study is to use simulations to quantify and understand the reductions in forward excursions, as well as liver and spleen loading, resulting from the application of pre-crash braking along with PPT.

II. METHODS

Global Human Body Models Consortium

The version 6.0 average male Global Human Body Models Consortium (GHBMC) detailed occupant model (M50-O_v6-0, release date 5 April 2021) [26] was used to study the response of liver and spleen. With a total of 2.57 million elements, the GHBMC model was chosen for its comprehensive modelling of human inner organs. More specifically, the individually modelled organs have detailed anatomical geometry as well as appropriate material properties. Furthermore, extensive validation, ranging from isolated body regions to full-body level in various load cases, made it the suitable choice for this study [26]. Active muscle control was deactivated, and the passive version of the occupant model was used, and the bone fracture was also disabled for this study.

Model of Sled Environment

Given the longer duration required to simulate both pre-crash and crash phases together, especially with the computationally intense detailed GHBMC model, it was decided to use a simplified sled model. Additionally, we sought to use a sled model that had been validated in combination with the GHBMC model. The model that was available for lateral load case in the GHBMC full-body model validation database [27] met our criteria. Although the original sled model was created for the lateral load case, the sled structural details, including seat-pan and

backrest, as well as the anchorage positions, were suitable for the frontal load case. Therefore, it was easily adapted for the purposes of the current study.

The sled environment model utilised in this study is displayed in Fig. 1 (shown on the left side). It consisted of a simplified sled model of rigid seat fixture [27] having a rigid floor and seat structure that included a headrest, backrest and seat-pan, each covered with a 60 mm layer of low-density foam. The seat backrest was reclined at 22 degrees from vertical, while the seat-pan was elevated 18 degrees from horizontal. The occupant model was positioned in an upright posture and restrained by a standard three-point belt system. The belt was routed such that the shoulder belt was passing over the mid-sternum on the chest and the lap belt was passing below the Anterior Superior Iliac Spine (ASIS) points on the pelvis. The belt was meshed in combination of 2-dimensional (2-D) and 1-dimensional (1-D) elements. The 2-D belt elements were used where the belt was expected to contact the occupant model while 1-D elements were used to connect the 2-D belt portions (shoulder belt and lap belt) to the anchorages at B-pillar, buckle and anchor point. The connection between the shoulder and lap segments of the 1-D belt elements was created at the buckle position through a 1-D slipring element with a coefficient of friction of 0.19. The belt was modelled with seat-belt material (i.e. *MAT_SEATBELT). Most of the model settings, for example those related to contact definitions, were retained in this study. There were automatic-surface-to-surface contacts defined between the occupant model to the seat belt with a friction coefficient of 0.3 and between the occupant model to all the seat structures with a friction coefficient of 0.4.

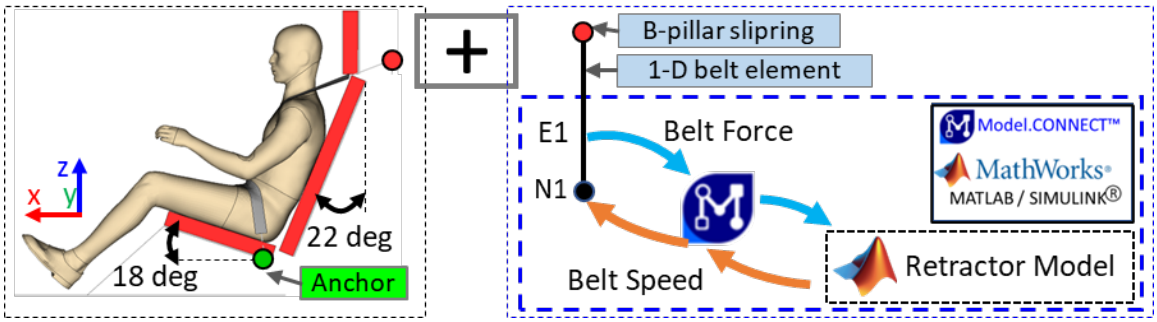

Fig. 1. Original sled model (on the left side) and modelling details of seat-belt systems (on the right side).

Seat-belt Systems

The original sled model was modified by adding a B-pillar-mounted shoulder retractor. A retractor model was connected to the shoulder belt 1-D element through a B-pillar slipring using a 1-D belt element (as seen in Fig. 1, right side). The retractor model consisted of a motorised pre-pretensioner (PPT), a pyro-pretensioner (RPT) and a 4 kN constant force load-limiter (LL). All the retractor functions were modelled in the Matlab/Simulink (The MathWorks, Natick, Massachusetts, United States). The Matlab/Simulink-based retractor model was then coupled to the sled model in the LS-DYNA using a third-party software Model.Connect™ (AVL List GmbH, Graz, Austria) The coupling provided a means to exchange the kinematics and kinetic information between the two solvers. While Matlab/Simulink solver controlled the belt pay-in/pay-out speed at the node N1, the force generated in the belt element E1 in the LS-DYNA solver was transferred back to the retractor model in Matlab/Simulink, thus forming a closed loop control system [28-29]. The retractor model, webbing material characteristics, and the complete belt system have been validated in-house to ensure they match the performance of their mechanical counterparts, both at the component level and the sub-system level. An exemplary result for system level validation of the retractor model is provided in the Appendix A1, Fig. A1.

The modular design of retractor functions in Matlab/Simulink allows for the activation or deactivation of a function to obtain the desired retractor configuration. In the current study, the retractor was used both with and without the motorised PPT. The motor parameters were based on the existing serial product configuration, which resulted in PPT force level of 350 N at the shoulder belt.

Simulation Conditions

Three cases of full-frontal impact at 56 kph were simulated, as detailed in Table I. The 0 g+0 N simulation represented both driving and impact at a speed of 56 kph without any activation of AEB or PPT. The other two simulations, 1 g+0 N and 1 g+350 N, included the AEB activation, resulting in an adjusted driving speed of 65

kph, along with PPT forces of 0 N (PPT not activated) and 350 N, respectively.

As illustrated in Fig. 2, each simulation had a total duration of 800 ms, which comprised an initial 300 ms for model stabilisation to achieve a force balance between the seat and the occupant model under the influence of gravity. The 0 g+0 N simulation prolonged this settling phase for an additional 300 ms before the 200 ms crash phase. In contrast, in the simulations with the AEB, a pre-crash braking of 300 ms was implemented, followed by the 200 ms crash phase. A shorter duration (300 ms) of 1 g AEB pulse with a ramp-up time of 100 ms was selected to gain efficiency on computation time while utilising the detailed GHBMC model. Although the 300 ms duration of the AEB pulse is on the lower limit of the range according to [30], we believe it is a conservative yet feasible choice and represents a reasonable compromise for this study.

The PPT was activated with the onset of the AEB pulse at 300 ms. The retractor pretensioner was activated 10 ms after the crash initiation, at 610 ms. Both the pre-crash and the crash phases were simulated in the same simulation run, without restarting the simulation. All the simulations were carried out using LS-DYNA MPP, single precision (R9.3.1, SVN 140922, LSTC/ANSYS, Livermore, CA, United States).

TABLE I
SIMULATION MATRIX

Simulation ID	Driving Speed (kph)	AEB activation time (ms)	Impact Speed (kph)	Pre-pretensioner force (N)
0 g+0 N	56	0	56	0
1 g+0 N	65	300	56	0
1 g+350 N	65	300	56	350

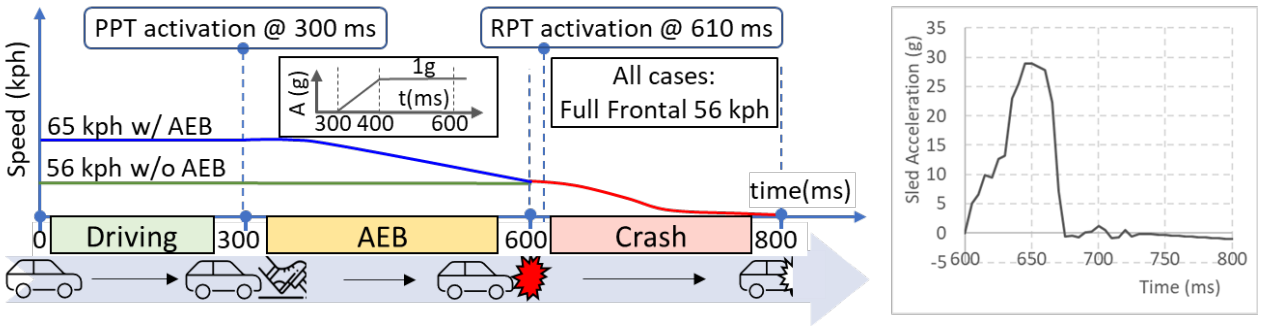

Fig. 2. Timeline of the pre-crash and crash events (on the left side) and the crash pulse (on the right side).

Result Analysis

The force at the upper shoulder belt (B3) and the retractor pay-in/pay-out was compared across the simulations. The occupant forward displacement relative to the sled was calculated at head centre of gravity (CoG), chest (at fourth thoracic vertebra (T4)) and pelvis CoG (shown in Fig. 3(a)).

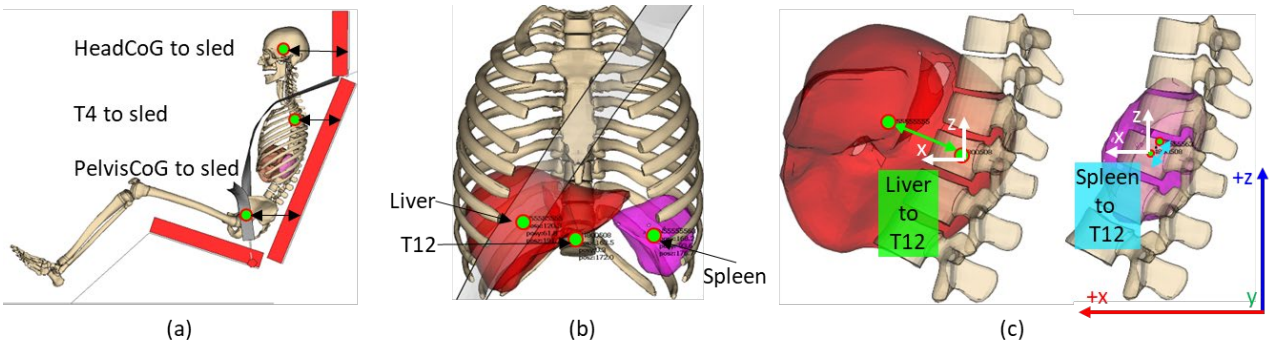

Fig. 3. (a) Displacements of head, T4 and pelvis CoGs with respect to sled; (b) CoG marker locations for liver, spleen and T12 with the shoulder belt; and (c) displacements of liver and spleen CoGs from T12.

The motion of liver and spleen was analysed for the simulated cases. However, the GHBMC model does not

have any pre-defined markers to compute their motion. We used the conventional method of defining *CONSTRAINED_INTERPOLATION type constraint in LS-DYNA. This method enabled us to interpolate the motion of a single dependent node from the motion of a set of independent nodes. Therefore, additional nodes were created at the CoGs of each of these organs and connected to the set of surface nodes of the corresponding part (as illustrated in Fig. 3(b)). To evaluate the loading on the liver and spleen, the X-direction acceleration of their CoG and the resulting a3ms-clip values were compared across simulations. Additionally, displacements of liver and spleen CoG relative to the pre-defined target at twelfth thoracic vertebra (T12) were analysed (as depicted in Fig. 3(c)), considering the proximity of their Z levels. To eliminate the organ displacements arising from spinal rotation during the occupant forward displacement, the organ displacements were computed with respect to T12 in the local coordinate system that was fixed at the CoG of T12 and initially aligned to the global coordinate system (see Fig. 3(c)).

Moreover, kinetic energy-based coupling-loss, as described by [31], was calculated for T4, liver and spleen and compared across simulations. This calculation measures the difference between the theoretical and the actual energy reduction of the occupant during a crash-induced deceleration. In an ideal scenario, when the occupant is optimally coupled to the car's deceleration, the energy path of the occupant will follow that of the car. A deviation from this represents a loss in coupling. A lower energy difference signifies a better coupling between the occupant and the car. A detailed exemplary calculation is provided in Appendix A2, Fig. A2.

III. RESULTS

Figure 4 and Fig. 5 shows the belt force and the retractor pay-in/out, respectively. In the pre-crash phase the belt force ramped-up earlier in the 1 g+350 N compared to the 1 g+0 N, but then reached to the same peak value at 425 N in both simulations. The PPT pulled in about 25 mm of belt in the 1 g+350 N simulation, whereas AEB without PPT resulted in 40 mm of belt pull-out in the 1 g+0 N simulation. The belt force and belt displacement remained almost zero in the 0 g+0 N simulation.

In the crash phase, the RPT (retractor pretensioner) activation caused the first peak in the belt force, with a higher peak force value in both the 1 g+350 N and 1 g+0 N simulations compared to the 0 g+0 N simulation (2.35 kN vs. 1.7 kN). Regardless of the differences in the belt geometries at 600 ms, the RPT pulled in approximately 35 mm of belt in all cases. Nevertheless, the maximum belt force reached 4 kN in all of the simulations, with a maximum belt payout of around 300 mm in the 0 g+0 N and 1 g+350 N simulations, and 330 mm in the 1 g+0 N simulation.

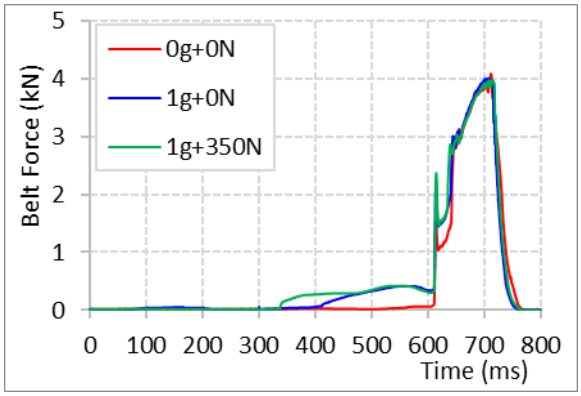

Fig. 4. Comparison of upper shoulder-belt force.

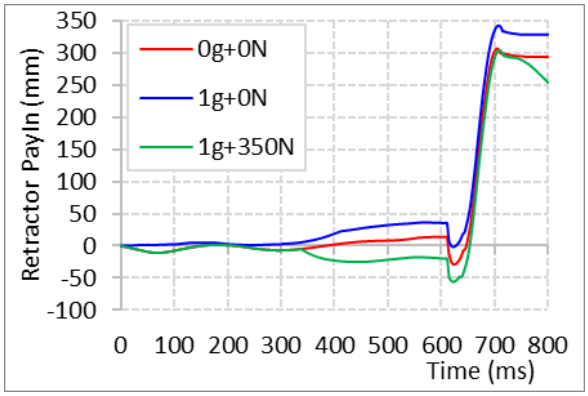

Fig. 5. Comparison of retractor displacement.

The forward excursion at Head CoG, T4 and Pelvis CoG is shown in Fig. 6 with timestamp markers indicating their positions at the end of the pre-crash phase at 600 ms. In the 1 g+0 N simulation, with AEB alone, the occupant was already displaced in a forward position at the beginning of the crash phase. On the other hand, in the 1 g+350 N simulation, the PPT force reduced the forward displacement during the pre-crash phase. For example, the chest position nearly matched to that in the 0 g+0 N simulation by the end of pre-crash phase and resulted in similar maximum forward displacement in the crash phase. The 1 g+0 N had the largest forward excursion compared to both 1 g+350 N and 0 g+0 N (e.g. 480 mm vs. 440 mm at the T4 CoG). Moreover, both AEB and PPT had minor effects on the pelvis forward displacement.

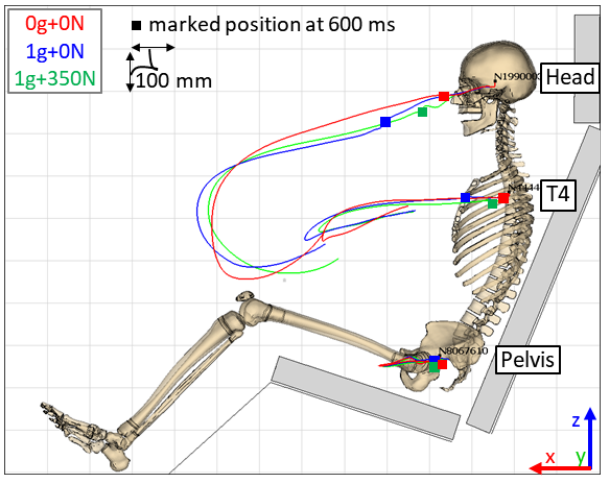

Fig. 6. Comparison of head, chest and pelvis trajectories relative to sled floor.

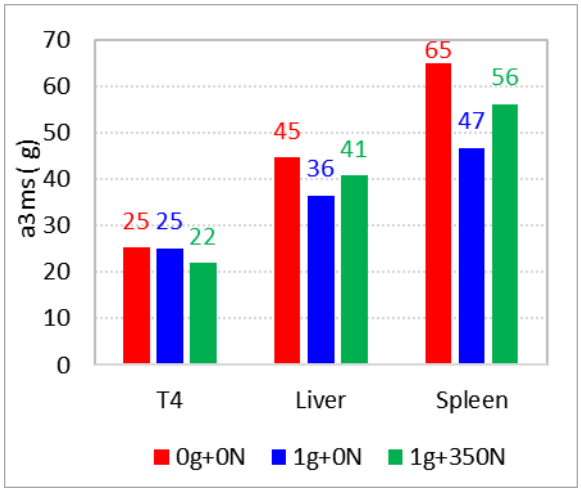

Fig. 7. Comparison of a3ms values calculated using X-acceleration for T4, liver and spleen.

Figure 7 shows comparison of a3ms-clip values obtained from the X-acceleration measurements of T4, liver and spleen. The highest acceleration was observed in both organs during the 0 g+0 N simulation, with the liver reaching 45 g and the spleen 65 g. The AEB-only simulation (1 g+0 N) showed reduced acceleration in both organs, with the liver at 36 g and the spleen at 47 g. In the 1 g+350 N simulation, where PPT force was applied, both organs experienced higher acceleration values, with the liver at 41 g and the spleen at 56 g. On the other hand, T4 acceleration remained relatively lower, ranging between 22 g and 25 g across all simulations. The X-acceleration time history plots are also provided in Appendix B.

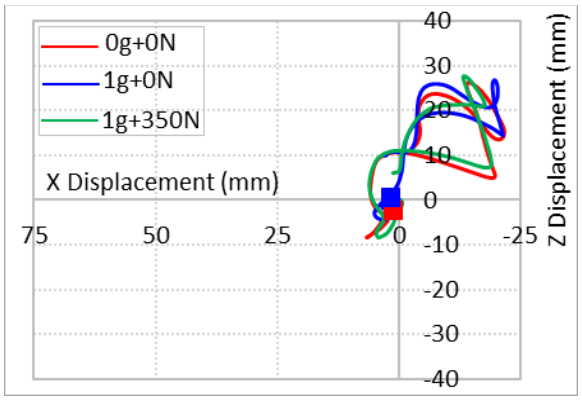

Fig. 8. Comparison of liver displacement relative to T12 in XZ plane, markers show position at 600 ms.

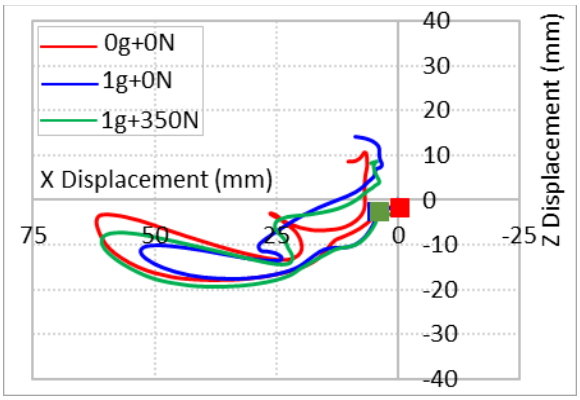

Fig. 9. Comparison of spleen displacement relative to T12 in XZ plane, markers show position at 600 ms.

Figure 8 and Fig. 9 show the displacement of liver and spleen relative to T12 in the XZ plane, respectively. The liver moved in the negative X- and positive Z-directions (towards and upwards to T12, respectively), whereas the spleen moved in the positive X- and negative Z-directions (away and downwards to T12, respectively). The liver X and Z displacements remained in the range of 20 mm to 25 mm in all simulations. The spleen experienced the highest X-displacement of 62 mm in the 0 g+0 N simulation, which reduced to 53 mm in the AEB-only simulation (1 g+0 N). However, in the 1 g+350 N simulation with PPT force, the displacement increased to 60 mm. The X- displacement and Z-displacement time history plots are also provided in Appendix C.

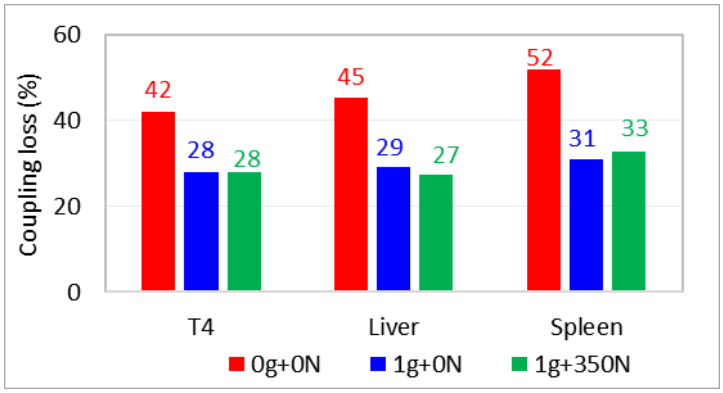

Fig. 10. Comparison of maximum coupling-loss for T4, liver and spleen.

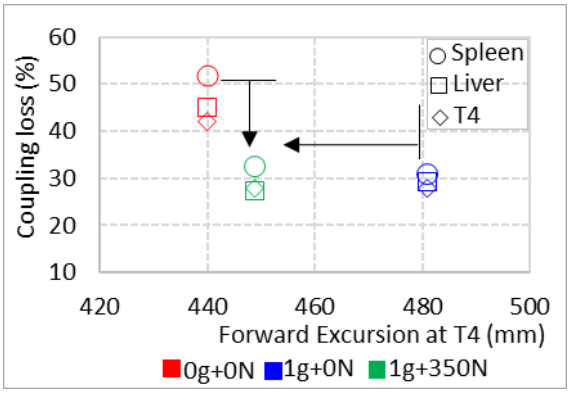

Fig. 11. Comparison of maximum coupling-loss for T4, liver and spleen as a function of maximum forward displacement of chest in X-direction.

Figure 10 shows the maximum value of coupling-loss for T4, liver and spleen. The highest coupling-loss was observed in the 0 g+0 N simulation, which decreased in the 1 g+0 N and 1 g+350 N simulations, indicating improved coupling with AEB and PPT activation. This trend was consistent for the three measured locations. Notably, the spleen showed the most substantial improvements, with coupling-loss decreasing from 52% in the 0 g+0 N simulation to 31% in the 1 g+0 N simulation. However, the activation of PPT in the 1 g+350 N simulation did not result in further improvements in spleen coupling, while it enhanced the liver coupling compared to the 1 g+0 N simulation. The coupling-loss time history plots are also provided in Appendix D. Finally, the coupling-loss and the maximum forward displacement at T4 are cross-plotted for the three simulated cases in Fig. 11. It shows that the combination of PPT and AEB not only improved the organ coupling, but also reduced the occupant forward displacement.

IV. Discussion

This study evaluated the effect of AEB and seatbelt PPT on the occupant forward displacement and abdominal organ response in full frontal car crashes by performing FE simulations with the detailed GHBMC model positioned in upright posture in a simplified sled environment.

When the AEB system was activated, the belt force in the pre-crash phase reached the same level in both with- and without-PPT simulations (i.e. 1 g+350 N and 1 g+0 N, respectively). However, there were differences in the restraining mechanisms. In the simulation without PPT (in 1 g+0 N), the initial slack in the belt allowed the occupant model to move forward freely under the AEB effect. The retractor was then locked and the belt firmly restricted the occupant motion. While the AEB kept pushing the occupant model forward against the resistance from the locked retractor, the belt pay out was increased due to the tightening of webbing on the spool and the stretching in webbing, resulting in more forward displacement. The belt force eventually balanced the inertial force by the end of the pre-crash phase; however, considerable forward displacement of the occupant model had already occurred.

In contrast, with PPT (in 1 g+350 N) the force exerted by PPT eliminated the initial slack and snugly fitted the belt on the occupant. When the AEB-induced inertial force further pushed the occupant model against the belt, the opposing PPT force prevented the occupant displacement. As a result, the occupant model was maintained nearly in the upright position. These restraining differences during the pre-crash phase consequently resulted in considerable differences in the maximum forward displacement of the occupant during the crash phase. These findings are in line with the previous studies [23-25][32].

This implies that a conventional retractor, without a PPT system, cannot retract the webbing and reduce the slack in the seatbelt during the pre-crash braking phase. As a result, the occupant may move forward depending upon the amount of slack in the belt system. Considering the real-life data, up to 75 mm slack [33] can be introduced into the shoulder belt due to poor seat-belt adjustment, bulky clothing, or webbing tightening in a locked retractor [34]. This can cause significant forward displacement, increasing the risk of serious injuries due to contact with interior structures, despite the AEB system reducing the severity of the crash [32][35]. An advanced retractor with a motorised pre-pretensioner can eliminate the slack in the seatbelt and thus minimize

forward movement of the occupant during pre-crash braking phase. Moreover, the activation strategy of PPT needs to be optimised relative to the AEB activation so as to remove the belt slack early in the process and prevent the occupant from moving forward.

It was observed that the application of the AEB alone (in 1 g+0 N) substantially reduced the peak acceleration experienced by both the liver and spleen during the crash phase compared to the no pre-crash braking (in 0 g+0 N) case. This decrease in peak acceleration indicates a reduction in loading on the organs when pre-crash braking was utilised. Moreover, the decline in coupling-loss suggests an improvement in the coupling for both organs. These findings are consistent with previous animal and volunteer sled test studies that reported protective benefits of pre-crash braking-induced inertial dynamic preload in the viscoelastic system of the human body [14-15]. While the increase in forward displacement resulting from pre-impact deceleration may not have been relevant to the objective of the above-mentioned sled studies, optimally controlling the occupant motion during car crashes has always been crucial in ensuring occupant safety. In that context, the current study confirmed the effectiveness of PPT in countering the occupant forward motion during pre-crash braking, as previously established by [23-25][32]. Moreover, the PPT force was able to reduce the inertial loading on both organs compared to the 0 g+0 N case (no pre-crash braking), but it was higher compared to the 1 g+0 N case. Nevertheless, it maintained the beneficial effects of AEB on enhancing the organ coupling during the crash phase, as summarised in Fig. 11.

In comparison to the liver, the spleen encountered higher loading and showed greater sensitivity to AEB and PPT applications. This may be attributed to differences in their displacements caused by variations in anatomy, interactions with surrounding organs, connecting tissues in the occupant model and the external parameter, such as belt loading. Despite being the largest and heaviest solid organ [36], the liver's location directly beneath the rib cage and just below the diaphragm in the abdominal cavity, as well as its anatomical connections with neighbouring tissues, restricted its overall movement. In addition, the shoulder belt, which was routed for the driver position, passed directly over the liver and forced it to move towards and upwards to the T12 during the restraining, as shown in Appendix E. This position of the belt directly above the liver may also explain the reason for improved coupling observed with the application of PPT, as the body regions directly under the diagonal belt are expected to couple more effectively than those further away from the belt.

Unlike the liver, the spleen was not restricted directly by any hard structure or by the belt in the front. Instead, it was located posterior and lateral to the stomach, a hollow organ modelled with an airbag definition in the GHBMC model. The interaction with the stomach appeared to affect the spleen response as it deformed during forward motion under acceleration loading, as demonstrated in Appendix F. Although these results cannot be directly substantiated, the overall kinematics and organ displacements are plausible when compared with the limited findings from cadaver tests. For example, it was reported that with the change in the cadaver orientation from the upright to inverted posture [8], liver markers moved between 71 mm and 192 mm due to gravity. This signifies that there is a significant potential for organs to move within the inter-abdominal space during high acceleration loading, such as in a vehicle crash.

There are several limitations in this study. The relevance of these results to real-life crash scenarios may be questionable, as the model only considers one occupant in an upright sitting position wearing a tightly fitted seatbelt with minimal slack. Future studies should consider various real-world factors, such as occupant variability, seating positions, AEB and crash pulses, restraint systems and their activation times, in order to understand the full range of the effectiveness of AEB and PPT on occupant safety. Notably, age and BMI should also be considered as they can considerably affect occupant forward displacements during braking, as highlighted by [37].

The selected ramp-up time of 100 ms for AEB deceleration to reach the peak value of 9.81 m/s2, resulted in a jerk of 98 m/s3. This jerk value is 60% higher than that reported in a study [20] involving pneumatic actuated braking via the brake pedal. It remains uncertain whether modern state-of-the-art braking systems can offer such higher rate of deceleration. Nevertheless, sensitivity of the ramp-up time should be investigated in the future.

Using a simplified sled environment model instead of a vehicle model with relevant interior structures poses another limitation in this study. Therefore, it should not be directly associated with any specific seating configuration. It does not represent a front seat configuration as it lacks components such as an airbag, steering column, and instrument panel. Interaction with the vehicle interior, particularly with airbag and steering wheel

for a driver position, are known to affect the loading on the forward-moving occupant in frontal crashes. Therefore, absence of these interactions in this study for the occupant model is expected to affect the results. Furthermore, the sled model does not represent a rear-seat configuration due to differences in seat geometry and the absence of interaction with the back of the front seat structure. Thus, caution should be exercised when interpreting the current findings in the context of the front and rear seat configurations. However, gaining computational efficiency was important, therefore using a simplified environment was an acceptable compromise.

Several studies [20] [23-25] have reported that occupant pre-crash responses are affected by muscle activation. However, muscle activation was not included in the current study for several reasons. Firstly, the active muscles in the detailed version of GHBMC model has not been validated specifically for the pre-crash applications. Although the simplified GHBMC model with active muscles has been validated for low-speed frontal crashes, it lacks the detailed abdominal model required for the current study. Additionally, it remains unclear how muscle forces from the simplified model can be adapted to the detailed model. Secondly, it is important to highlight that previous studies utilizing active muscles in HBMs have raised concerns regarding the reliability of muscle forces, particularly during the crash phase [20, 23-25], despite muscle force levels were validated for the pre-crash phase. Postural control algorithms are commonly used in HBMs including in GHBMC, for regulating the active muscle forces. It has been noted that these algorithms tend to generate higher levels of muscle activations during the crash phase. Unfortunately, lack of data for validating HBM muscle response during the crash phase leads to additional uncertainty. Lastly, the aim in the current study was to capture general trends and relative differences in organ loading resulting from pre-crash AEB activation along with pre-pretensioner, rather than focusing on absolute values. Therefore, it is not expected that the observed trends in organ loading patterns based on the passive GHBMC model would differ considerably from that of active version of the model.

Another limitation is related to the occupant model itself, specifically to the validity of the organ response for the crash loading. The GHBMC model represents human abdominal organs to detailed level, both in terms of geometry and material characterisation, and it has been extensively validated for different types of frontal or oblique loading scenario [26]. However, these validations are typically limited to the global response of the abdomen where only externally applied forces and the resulting displacements were compared. None of these load cases could validate the model regarding the kinematics or the strain response of the internal abdominal organs [13]. Lately, kinematic responses of the liver in scaled versions of GHBMC M50 model were compared to the liver responses recorded in the tests using ultrafast ultrasound imaging during abdominal impact on human cadavers [13]. It was reported that some of the experimental trends could be reproduced in the simulations (e.g. initial angle) while others differed more widely (e.g. final caudal motion). Particularly, both X-direction and Z-direction peak displacements of the liver in the simulations followed the same trend as in the tests, but their amplitudes were overestimated. This indicates that the model requires further improvements, specifically to enhance the local level responses of the abdominal organs. This underlines the need for more research on organ loading in the future.

V. CONCLUSIONS

This study attempted to quantify and understand the effects of PPT on forward excursion due to AEB and the consequences for the inertial loading on abdominal organs. While each effect has been studied independently in the past, their combined effects were evaluated in the current study using an advanced Human Body Model as a tool. It was found that a conventional belt system (without PPT) was not capable of reacting to the AEB and thus did not prevent the occupant from moving forward, but it did reduce the inertial loading on the liver and spleen in 1 g+0 N. Adding a 350 N PPT in 1 g+350 N counteracted the occupant's forward motion during pre-crash and held it in upright posture before the crash. It reduced the inertial loading on both organs against the 0 g+0 N case and maintained the organ coupling in the crash at an equivalent level to that in the 1 g+0 N case. Therefore, it can be concluded that PPT appears to reduce the abdominal organ loading without compromising forward excursion. However, further research on organ loading should be conducted.

VI. ACKNOWLEDGEMENTS

The authors would like to express their sincere gratitude to James H. Raddin, Bernard F. Hearon and James

W. Brinkley for their invaluable research on the dynamic preload effects. A special note of appreciation to Bernard F. Hearon for providing valuable insights and the reference papers that were extremely helpful.

VII. REFERENCES

[1] Campbell, B. J. (1987) Safety belt injury reduction related to crash severity and front seated position. *Journal Trauma*, **27**: pp.733–739.

[2] Evans, L. (1996) Safety-belt effectiveness: the influence of crash severity and selective recruitment. *Accident Analysis & Prevention*, **28**: pp.423–433.

[3] Biss, D. J. (1988) Safety performance evaluation of slack effects in three-point safety belts using the Hybrid III dummy in frontal and frontal oblique sled tests. *Proceedings of 16th Annual Workshop on Human Subjects for Biomechanical Research*, 1988, pp.69–114.

[4] Kahane, C. (2013) Effectiveness of pretensioners and load limiters for enhancing fatality reduction by seat belts. NHTSA, DOT HS 811 835, November 2013.

[5] Pipkorn, B., Wass, J. (2017) Pre-crash triggered pretensioning of the seat belt for improved safety. *Proceedings of the ESV Conference*, 2017, Paper Number 17-0104.

[6] Jamison, C. E., Marangoni, R. D., Glaser, A. A. (1968) Viscoelastic properties of soft tissue by discrete model characterization. *Journal of Biomechanics,* **1**(1): pp.33–36.

[7] Beillas, P., Lafon, Y., Smith, F. W. (2009) The effects of posture and subject-to-subject variations on the position, shape and volume of abdominal and thoracic organs. *Stapp Car Crash Journal,* **53**: p.127.

[8] Howes, M. K., Hardy, W. N., Beillas P. (2013) The Effects of cadaver orientation on the relative position of the abdominal organs. *Annals of Advances in Automotive Medicine*, **57**: pp.209–224.

[9] Nicolas, C., Thierry, S., *et al.* (2006) Biomechanics study of the human liver during a frontal deceleration. *The Journal of Trauma*, **61**: pp.855–61.

[10] Howes, M. K., Gregory, T. S., Hardy, W. N., Beillas, P. (2012) Kinematics of the thoracoabdominal contents under various loading scenarios. *Stapp Car Crash Journal*, **56**: pp.1–48.

[11] Howes, M. K., Hardy, W. N., Beillas P. (2013) The Effects of cadaver orientation on the relative position of the abdominal organs. *Annals of Advances in Automotive Medicine,* **57**: pp.209-224.

[12] Howes, M. K., Hardy, W. N., Agnew, A. M., Hallman, J. J. (2015) Evaluation of the kinematic responses and potential injury mechanisms of the jejunum during seatbelt loading. *Stapp Car Crash Journal*, **59**: pp.225–267.

[13] Le Ruyet, A., Berthet, F., Rongiéras, F., Beillas, P. (2016) Effect of abdominal loading location on liver motion: experimental assessment using ultrafast ultrasound imaging and simulation with a human body model. *Society of Automotive Engineers Technical Paper*, 2016, 2016-22-0003.

[14] Raddin, J. H. Jr, Brinkley, J. W., Hearon, B. F. (1980) The Implications of dynamic preload in human impact tolerance. *Presented at the 51st Annual Scientific Meeting of the Aerospace Medical Association*, 1980, Anaheim, California.

[15] Hearon, B. F., Raddin, J. H. Jr, Brinkley, J. W. (1982) Evidence for the utilization of dynamic preload in impact injury prevention. *Presented at the 51st Annual Scientific Meeting of the Aerospace Medical Association*, May 1982.

[16] Baumann, K-H, Justen, R., Schöneburg, R. (2001) A Vision for an integrated safety concept. *Proceedings of the ESV Conference*, 2001, Amsterdam, Netherlands, Paper 01-493.

[17] European New Car Assessment Programme (Euro NCAP) Assessment Protocol – Safety Assist Version 9.0.3.

[18] Fildes, B., Keall, M., *et al*. (2015) Effectiveness of low-speed autonomous emergency braking in real-world rear-end crashes. *Accident Analysis & Prevention*, **81**: pp.24–29.

[19] Cicchino, J. B. (2017) Effectiveness of forward collision warning and autonomous emergency braking systems in reducing front-to-rear crash rates. *Accident Analysis & Prevention,* **99**: pp.142–152.

[20] Schoeneburg, R., Baumann, K-H, Fehring, M., Ag, D., Cars, M. (2011) The efficiency of PRE-SAFE systems in pre-braked frontal collision situations. *Proceedings of the ESV Conference*, 2011, Washington, DC, 11–0207.

[21] Yamada, K., Gotoh, M., Kitagawa, Y., Yasuki, T. (2016) Simulation of occupant posture change during autonomous emergence braking and occupant kinematics in frontal collision. *Proceedings of the IRCOBI Conference*, 2016, Malaga, Spain, pp.261–274.

[22] Boyle, K., Fanta, A., *et al*. (2020) Restraint systems considering occupant diversity and pre-crash posture. *Traffic Injury Prev*ention, **21**: pp.S31–S36.

[23] Mages, M., Seyffert, M., Class, U. (2011) Analysis of the Pre-crash Benefit of Reversible Belt pre-pretensioning in different accident scenarios. *Proceedings of the ESV Conference*, 2011, Washington, DC.

[24] Mishra, E., Mroz, K., Pipkorn, B., Lubbe, N. (2022) Effects of automated emergency braking and seatbelt pre-pretensioning on occupant injury risks in high-severity frontal crashes. *Frontiers in Future Transportation, Sec. Transport Safety*, Volume 3. https://doi.org/10.3389/ffutr.2022.883951.

[25] Östh, J., Brolin, K., Bråse, D. (2015) A human body model with active muscles for simulation of pretensioned restraints in autonomous braking interventions. *Traffic Injury Prevention*, **16**: pp.304–313.

[26] GHBMC M50-O Documentation Users' Manual 2021, Global Human Body Models Consortium, LLC.

[27] Cavanaugh, J. M. (1990) Biomechanical response and injury tolerance of the thorax in twelve sled side impacts. *Stapp Car Crash Journal*, 34th, Orlando, Florida, USA.

[28] Schilling, S., Soni, A., *et al.* (2021) Coupling feedback control loop-based model in Simulink to finite element model in LS-Dyna: Application to reposition forward leaning occupant to upright posture. *Proceedings of the 13th European LS-DYNA Conference*, 2021.

[29] Schilling, S., Soni, A., *et al*. (2022) Evaluation of motorized seatbelts in the Euro NCAP AEB-CCFtap scenario: Application of a feedback control loop model in Simulink coupled to a finite element model in LS-Dyna. *Fahrzeugsicherheit-2022*, pp.295–312.

[30] Spitzhüttl, F., Liers, H. (2019) Calculation of the point of no return (PONR) from real-world accidents. *Proceedings of the ESV Conference*, 2019, Paper Number 19-0141.

[31] Zellmer, H., Kahler, C. K., Burkhard, E. (2005) Optimized pretensioning of the belt system: a rating criterion and the benefit in consumer tests. *Proceedings of the ESV Conference*, 2005, Paper Number 05-0004-O.

[32] Woitsch, G., Sinz, W. (2014) Influences of pre-crash braking induced dummy–forward displacements on dummy behavior during EuroNCAP frontal crash test. *Accident Analysis & Prevention*, **62**: pp.268–275.

[33] Ciccone, M., Wells, J. (1988) Improper shoulder belt use by Maryland drivers, *HUMAN FACTORS*, **30**(3): pp.359–366.

[34] Bacon, D. (1989) The effect of restraint design and seat position on the crash trajectory of the Hybrid III dummy, in Hybrid III: The first human like crash test dummy. *Society of Automotive Engineers*, 1989, Warrendale, PA, pp.641–647.

[35] Bose, D., Crandall, J. R., Untaroiu, C. D., Maslen, E. (2008) Influence of pre collision occupant properties on the injury response during frontal collision. *Proceedings of the IRCOBI Conference*, 2008, Bern, Switzerland, pp.135–147.

[36] Gholamzadeh, S., Zarenezhad, M., Montazeri, M. (2017) Statistical analysis of organ morphometric parameters and weights in South Iranian adult autopsies. *Medicine (Baltimore)*, **96**(21): p.e6447.

[37] Reed, M. P., Ebert, S. M., *et al*. (2018) Passenger head kinematics in abrupt braking and lane change events. *Traffic Injury Prevention*, **19**: pp.S70–S77.

VIII. APPENDIX

Appendix A1: Validation of Retractor Model: Exemplary Results

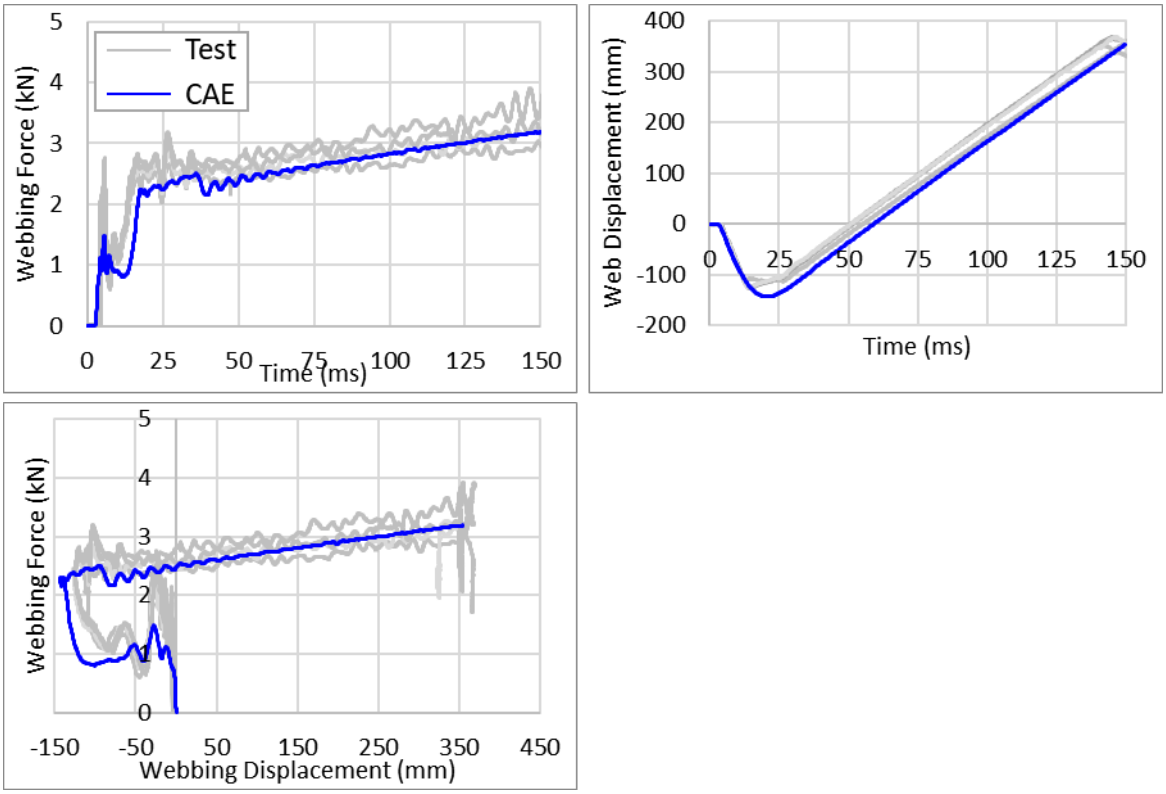

Fig. A1. Upper Left: Webbing force time history, Upper Right: Webbing displacement time history and Lower Left: Webbing force over displacement.

Appendix A2: Coupling-Loss: Exemplary calculation

- Coupling Loss calculation
  - Velocity profile of sled and T4
  - Energy density calculation
    - $\frac{E}{m} = \frac{1}{2}v^2$
  - Relative Energy density
    - $e_{rel} = \frac{\left[\frac{E}{m}\right]_t}{\left[\frac{E}{m}\right]_{t=0}} * 100$
  - Coupling loss
    - $T4_{e_{rel}} - Sled_{e_{rel}}$

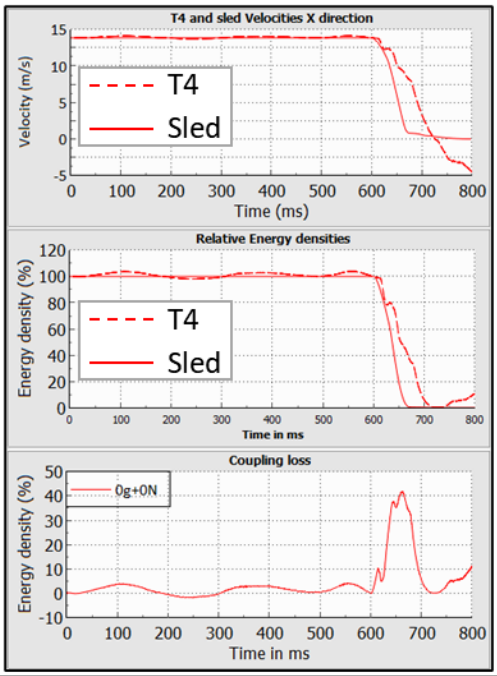

Fig. A2. Description of Coupling-Loss with an exemplary calculation for 0 g+0 N case for T4 location; the same calculation was performed for the liver and the spleen.

Appendix B: Plots of x-acceleration time histories for liver, spleen and T4

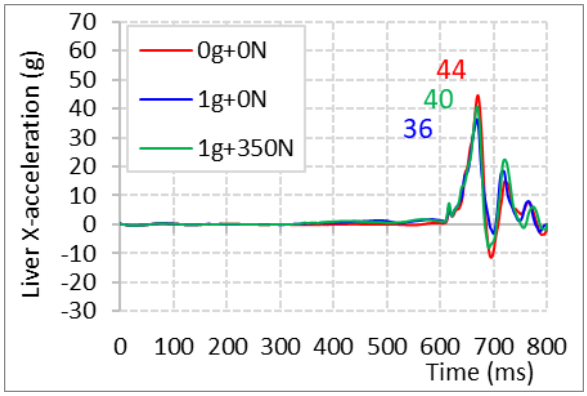

Fig. B1. Comparison of X-acceleration for liver with peak values.

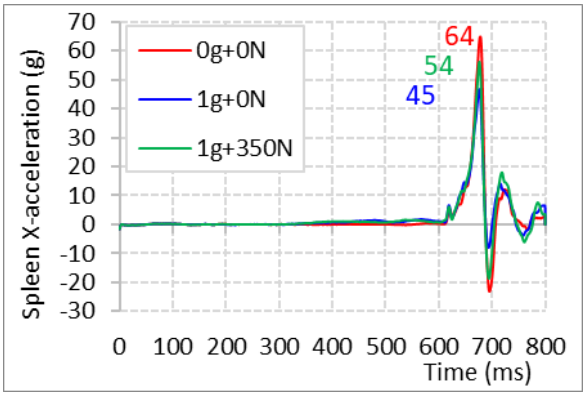

Fig. B2. Comparison of X-acceleration for spleen with peak values

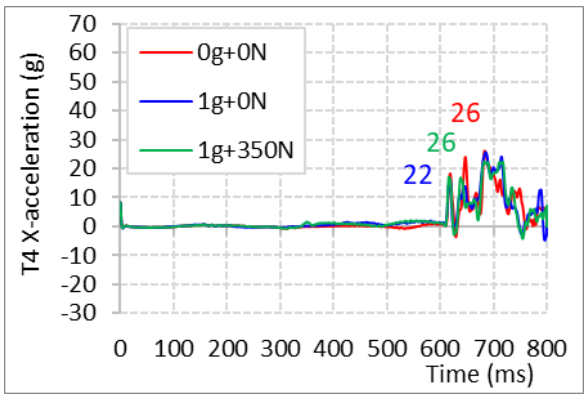

Fig. B3. Comparison of X-acceleration for T4 with peak values.

Appendix C: Plots of displacement time histories relative to T12 in X- and Z-directions for liver and spleen

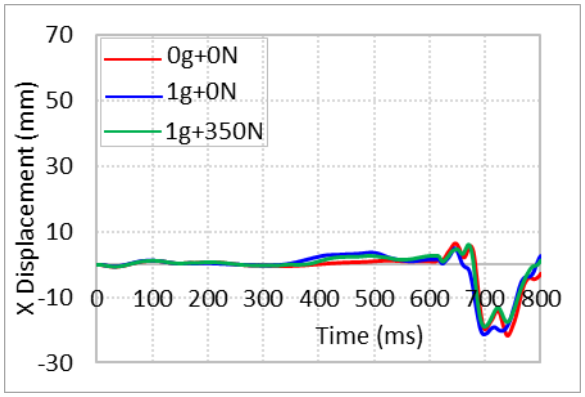

Fig. C1. Comparison of liver displacement relative to T12 in X-direction.

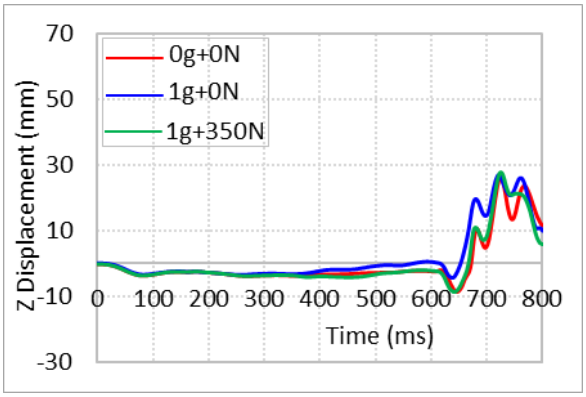

Fig. C2. Comparison of liver displacement relative to T12 in Z-direction.

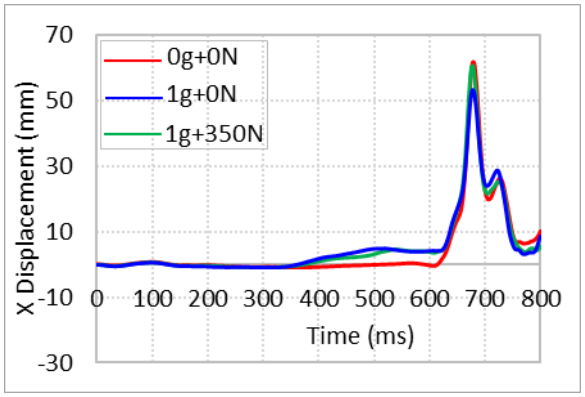

Fig. C3. Comparison of spleen displacement relative to T12 in X-direction.

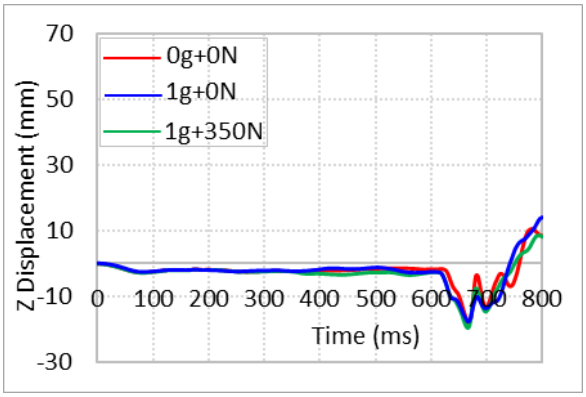

Fig. C4. Comparison of spleen displacement relative to T12 in Z-direction.

Appendix D: Plots of coupling-loss time histories for liver and spleen

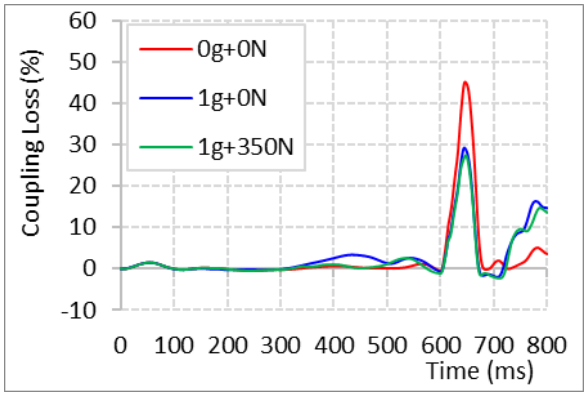

Fig. D1. Comparison of coupling-loss for liver.

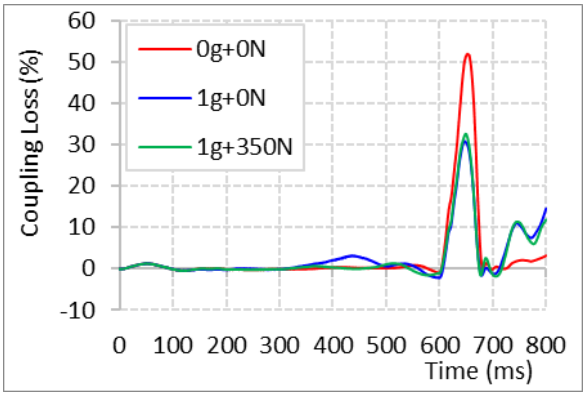

Fig. D2. Comparison of coupling-loss for spleen.

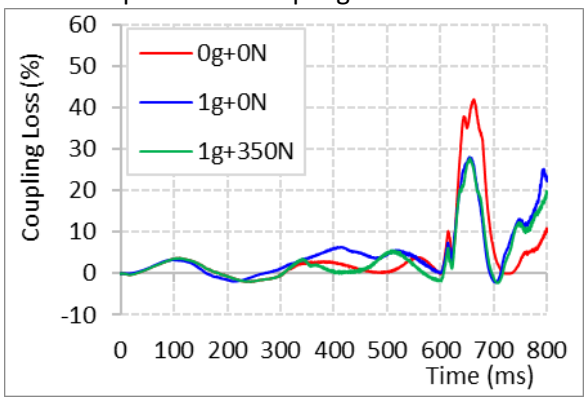

Fig. D3. Comparison of coupling-loss for T4.

Appendix E: Liver position at the time of maximum Z-displacement relative to T12 for different simulations

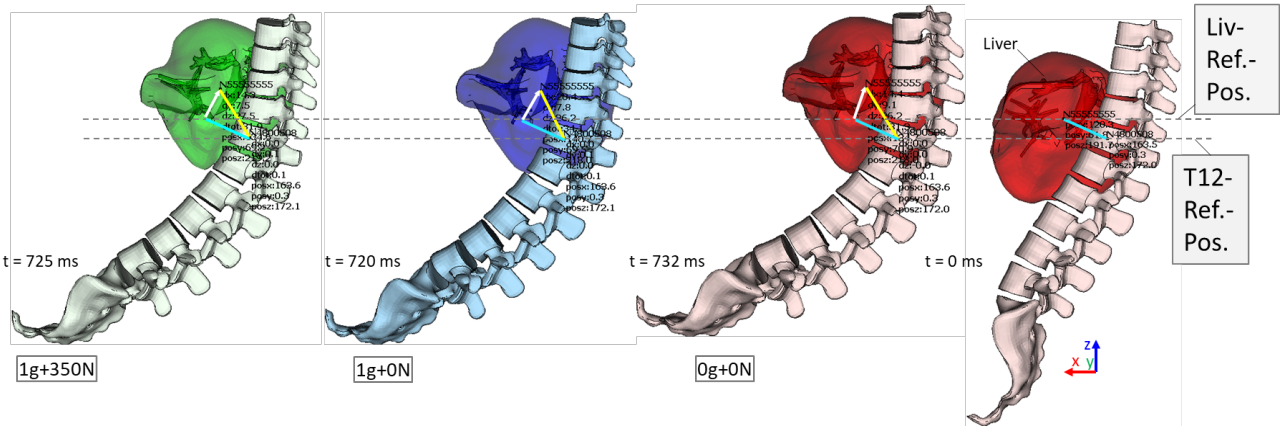

Fig. E1. Comparison of deformation and position of liver CoG relative to T12 CoG for different simulations at the time of respective maximum Z-displacement. The motion of T12 vertebra was locked in the animations to draw the model positions.

Note:

1) Other parts are not shown for better visualisation.

2) Model position at time t = 0 ms is same for all the simulations and therefore only one case is shown (the right most).

Appendix F: Spleen position at the time of maximum X-displacement relative to T12 for different simulations

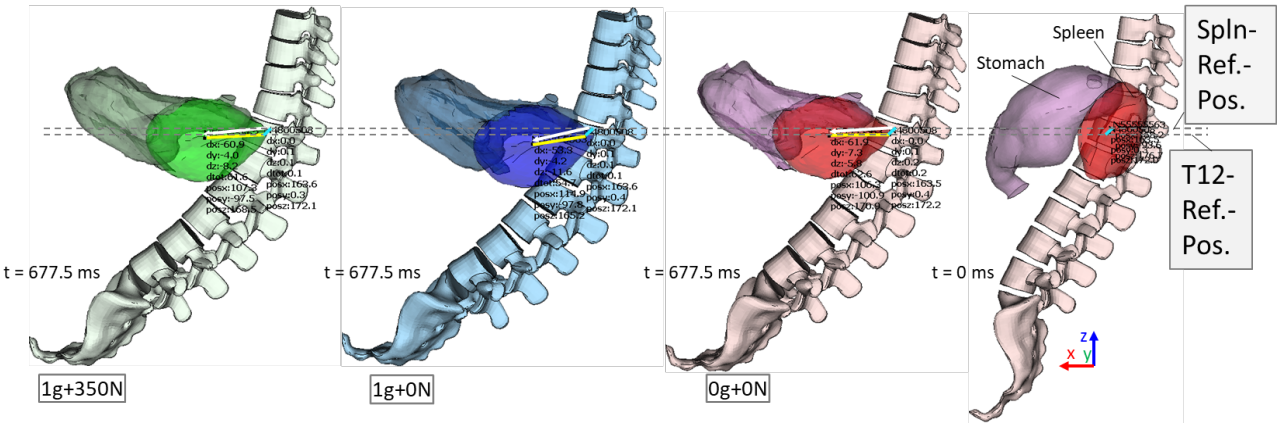

Fig. F1. Comparison of deformation and position of spleen CoG relative to T12 CoG for different simulations at the time of respective maximum X-displacement. The stomach is shown here to demonstrate interaction with the spleen. The motion of T12 vertebra was locked in the animations to draw the model positions.

Note:

1) *Other parts are not shown for better visualisation.*
2) *Model position at time t = 0 ms is same for all the simulations and therefore only one case is shown (the right most).*